Combining DPG in space with DPG time-marching scheme for the transient advection-reaction equation

Judit Muñoz-Matute[a,b], Leszek Demkowicz[b], Nathan V. Roberts[c]

[a] *Basque Center for Applied Mathematics (BCAM), Bilbao, Spain*
[b] *Oden Institute for Computational Engineering and Sciences, The University of Texas at Austin, USA*
[c] *Center for Computing Research, Sandia National Laboratories, Albuquerque, New Mexico, USA*

We dedicate this work to Prof. J. Tinsley Oden on the occasion of his 85th birthday

Abstract

In this article, we present a general methodology to combine the Discontinuous Petrov-Galerkin (DPG) method in space and time in the context of methods of lines for transient advection-reaction problems. We first introduce a semidiscretization in space with a DPG method redefining the ideas of optimal testing and practicality of the method in this context. Then, we apply the recently developed DPG-based time-marching scheme, which is of exponential-type, to the resulting system of Ordinary Differential Equations (ODEs). We also discuss how to efficiently compute the action of the exponential of the matrix coming from the space semidiscretization without assembling the full matrix. Finally, we verify the proposed method for 1D+time advection-reaction problems showing optimal convergence rates for smooth solutions and more stable results for linear conservation laws comparing to the classical exponential integrators.

Keywords: DPG method, ultraweak formulation, optimal test functions, exponential integrators, method of lines, advection-reaction equation

1. Introduction

The Discontinuous Petrov-Galerkin (DPG) methodology was introduced twelve years ago as a discretization method to solve steady-state convection problems [8] employing a marching strategy, solving the problem in mesh layers from the inflow boundary to outflow. The authors proved optimal convergence and approximation properties comparing to the classical Discontinuous-Galerkin (DG) method. Since then, the DPG method has been applied to a wide variety of problems [10, 13, 16, 24, 28, 35] and has been analyzed over the years by several authors [3, 5, 6, 9]. Recently, Demkowicz and Roberts revisited the method for advection-reaction problems in [17]. We can summarize the general idea behind DPG as follows: it is a discretization method that computes optimal test functions in order to ensure the discrete stability of the problem. One of the most interesting features is that it can be

reinterpreted as a minimum residual method leading to an error representation function, which is the Riesz representation of the residual, the norm of which can be computed locally and used to drive adaptivity [12, 15, 34].

Recently, we went back to the roots of the method and published a series of articles [30–32] where we extrapolated the ideas of the original DPG work for convection problems to transient Partial Differential Equations (PDEs). The main motivation was that in the context of the method of lines, after semidiscretization in space of a PDE by a Galerkin method, we obtain a system of Ordinary Differential Equations (ODEs) as follows

$$\begin{cases} U'(t) + AU(t) = F(t), \ \forall t \in [0,T], \\ U(0) = U_0, \end{cases} \tag{1}$$

which is essentially a convection-reaction problem in 1D. Although there are previous works on DPG method for transient problems – in the context of space-time [14, 18–20, 23] and finite differences in time together with DPG in space [21, 22, 36] – our perspective was the first one to regard the DPG method itself as a time-integration scheme. Our approach has several appealing benefits, including the simplicity of implementation, unconditional stability and an error representation for adaptivity. The main drawback compared to the space-time approach is that we cannot perform local space-time refinements.

To develop our DPG-based time-marching scheme we first consider a broken ultraweak variational formulation of system (1) introducing new unknowns at each time step (traces). Then, we fix a discrete trial space and we compute the corresponding optimal test functions analytically considering a localizable adjoint norm for the test space. The latter is possible in this context because it is a 1D problem. We proved in [32] that the optimal test functions are exponential-related functions of the matrix A that satisfy the adjoint equation and, therefore, they completely decouple the trace variables from the interiors. In the resulting time-marching scheme we obtain an equation to compute the traces in time (which is equivalent to classical exponential integrators [25–27]) and an additional system to compute the field variables. We proved that our method delivers the L^2-projection of the analytical solution in the element interiors in time.

The coupling of our DPG time-marching scheme with a Bubnov-Galekin method was straightforward for symmetric variational formulations in space. We then asked ourselves the natural question of how to semidiscretize a non-symmetric and/or non-coercive variational problem with the DPG method in space to obtain a system like (1) and then apply the time-stepping. The key to answering this question was to decouple the idea of optimal testing in space from optimal testing in time. In this work, we answer this question for the transient advection-reaction problem in 1D+time.

We present the semidiscretization in space in three steps that correspond to our original thinking and how we overcome several limitations:

1. We first consider a conforming ultraweak variational formulation of the problem in space. We select the natural Petrov-Galerkin discretization in this case that consists of discontinuous piecewise polynomials of order p for trial and H^1-conforming polynomials of order $p+1$ vanishing on the outflow boundary. The motivation behind this

setting is that we know from [8] that this choice of spaces corresponds to the optimal testing in the DPG method for pure advection problems in 1D. However, this choice is not generalizable to higher dimensions and it is no longer optimal for other operators.

2. Motivated by step 1, the second step is to introduce the idea of optimal testing that symmetrizes the spatial operator together with a broken ultraweak variational formulation which is critical to obtain a practical method. Therefore, we introduce interface variables that are, like the fields variables, time-dependent. Finally, as in the classical DPG method, we have two types of optimal test functions and statically condensing the trace variables we obtain a system like (1). However, we obtain a matrix A that is no longer sparse and it is therefore not practical to compute the exponential-like functions with existing algorithms [1, 4, 29, 33].

3. Finally, we redefine the concept of the "practical DPG method" in this context. We show in Section 3 that we need to consider optimal test functions that are orthogonal to the mass matrix in order to obtain a matrix A that only involves the inversion of matrices at the element level.

We show in the numerical results that we obtain optimal convergence rates both in space and time with this method in combination with the DPG time-marching scheme. Moreover, the method presented in this article captures the evolution of transport problems with non-smooth initial data. In conclusion, we present in this article a general methodology of combining a DPG semidiscretization in space together with exponential-related methods in time. The method is practical in the computational sense and it can easily be generalized to higher dimensions and to other problems.

The article is organized as follows: Section 2 presents the 1D+time model problem we consider in this work. In Section 3 we introduce the semidiscretization in space by three methods: a classical Petrov-Galerkin method, a DPG method and a practical DPG method. We also introduce the test norms we employ to compute the optimal test functions in space. Section 4 provides an overview of the time-marching scheme we developed in our previous works [31, 32] and some comments about how to efficiently compute the exponential of the matrix coming from the space semidiscretization employing existing software. Section 5 proves the consistency of our DPG time-marching approach with steady state solutions. In Section 6 we present the numerical results for 1D+time advection-reaction problems with different regularity in the data. Section 7 summarizes the conclusions and future research lines. Finally, in Appendix A we state the problem of selecting the adjoint graph norm for pure advection problems and in Appendix B we explain how to obtain the system to compute time-dependent traces.

2. Model problem

Let $I = (0, T)$ with $T > 0$ and $\Omega = (0, 1)$; we consider the 1D+time advection-reaction equation

$$\begin{cases} u_t(x,t) + bu_x(x,t) + cu(x,t) = f(x,t), & \text{in } \Omega \times I, \\ u(0,t) = g(t), & \text{in } I, \\ u(x,0) = u_0(x), & \text{in } \Omega. \end{cases} \tag{2}$$

where b and c are constants and $f \in L^2(I; L^2(\Omega))$, $g \in L^2(I)$, $u_0 \in L^2(\Omega)$. We are interested in solutions with space-time discontinuities, for example, a discontinuous initial condition u_0 that propagates in time. In order to capture those discontinuities, we consider ultraweak variational formulations both in space and time in the spirit of the *Method of Lines* [37], i.e., we discretize in space first and then we discretize the resulting system of Ordinary Differential Equations (ODEs) in time.

3. Semidiscretization in space

In this section, we focus on the semidiscretization in space of problem (2). We consider a mesh Ω_h of Ω

$$0 = x_0 < x_1 < \ldots < x_{n-1} < x_n = 1, \tag{3}$$

and we define $\Omega_i = (x_{i-1}, x_i)$, $h_i = x_i - x_{i-1}$, $\forall i = 1, \ldots, n$ and $h = \max_{1 \le i \le n} h_i$. We denote by Γ_h the mesh skeleton and $\mathcal{P}^p(\Omega_h)$ the space of piecewise polynomials up to order p defined in Ω_h. In the notation throughout the article we omit the dependence on the space variable but we maintain the dependence upon time, i.e., we denote $u(t) := u(x,t)$.

We first introduce in Section 3.1 an ultraweak Petrov-Galerkin formulation in space which is only valid for 1D problems. We then introduce in Section 3.2 our DPG formulation in space which can be extended to arbitrary space dimensions and any operator but is not practical for the computation of the exponential. Finally, in Section 3.3 we present our final practical DPG formulation.

3.1. PG formulation

We consider test functions in $H^1(\Omega)$ vanishing on the outflow boundary

$$H^1_+(\Omega) := \{v \in H^1(\Omega) \mid v(1) = 0\},$$

and by integration by parts, we introduce the following ultraweak variational formulation in space

$$\begin{cases} \text{Find } u \in C^1(\bar{I}; L^2(\Omega)) \text{ s.t. } \forall t \in \bar{I} \\ \quad (u_t(t), v) + \mathfrak{b}(u(t), v) = \tilde{f}(t, v), \quad \forall v \in H^1_+(\Omega), \\ \quad (u(0), w) = (u_0, w), \quad \forall w \in L^2(\Omega). \end{cases} \tag{4}$$

where $(\cdot, \cdot)$ denotes the $L^2(\Omega)$ inner product and

$$\mathfrak{b}(u(t), v) := (u(t), -bv_x + cv), \quad \tilde{f}(t, v) := (f(t), v) + g(t)bv(0) \tag{5}$$

A natural choice for discretizing (4) is

$$\begin{cases} \text{Find } u_h \in C^1(\bar{I};\mathcal{U}_h) \text{ s.t. } \forall t \in \bar{I} \\ (u_{h,t}(t), v_h) + \mathfrak{b}(u_h(t), v_h) = \tilde{f}(t, v_h), \qquad \forall v \in \mathcal{V}_h, \\ (u_h(0), w_h) = (u_0, w_h), \quad \forall w_h \in \mathcal{U}_h, \end{cases} \tag{6}$$

where

$$\mathcal{U}_h := \mathcal{P}^p(\Omega_h), \;\; \mathcal{V}_h := \mathcal{P}^{p+1}(\Omega_h) \cap H^1_+(\Omega). \tag{7}$$

Here, we have piecewise polynomials of order p for trial and globally continuous piecewise polynomials of order $p+1$ vanishing at the outflow boundary for test functions. We express the solution of (6) as a tensor product

$$u_h(x,t) = \sum_{j=1}^{s} u_{h,j}(t)\phi_j(x),$$

being $s := n(p+1) = \dim(\mathcal{U}_h)$, $\phi_j(x)$ the basis functions in $\mathcal{U}_h$. Note that both spaces have the same dimension and therefore, (6) reduces to the following square system of ODEs

$$\begin{cases} MU'(t) + KU(t) = \tilde{F}(t), \; \forall t \in \bar{I}, \\ M_0 U(0) = \tilde{U}_0, \end{cases} \tag{8}$$

where $U(t)$ is the vector containing the (time-dependent) degrees of freedom in space, $\tilde{F}(t)$ and $\tilde{U}_0$ are the vectors corresponding to the right-hand-side of (6), M and K are the mass and the stiffness matrices between spaces $\mathcal{U}_h$ and $\mathcal{V}_h$ and M_0 is the mass matrix corresponding to the trial space. In this case, the matrix A in (1) which we obtain for computing the exponential-related functions is

$$A = M^{-1}K. \tag{9}$$

We know from [8], that for the steady-state advection problem ($u' = f$) the optimal choice of spaces in the DPG setting is precisely (7) for the ultraweak variational formulation. We will see in the numerical results in Section 6 that this choice of symmetrizing the operator in space combined with the DPG time-marching scheme delivers superb solutions in the case of the transport problem ($c = 0$) with discontinuous initial conditions. However, this choice is only possible for one-dimensional problems as a similar selection in higher space dimensions would lead to a rectangular system of ODEs in (8).

3.2. DPG formulation

In the DPG methodology [11], the step of breaking the test spaces is crucial to obtain a practical method. On the other hand, the enrichment of the test space is essential to ensure the stability of the method. In this section, we introduce these ideas and the concept of optimal test functions in space for a broken ultraweak variational formulation of problem (2). We write $\mathcal{U} := L^2(\Omega)$ and $\mathcal{V} := H^1(\Omega_h)$, the H^1-broken space on the mesh Ω_h.

First, we integrate by parts in space and we introduce the time-dependent interface variables

$$\bar{u}^i(t) := u(x_i, t),\ \forall i = 1, \dots, n,$$

then we obtain

$$\begin{cases} \text{Find } u \in C^1(\bar{I}; \mathcal{U}) \text{ and } \bar{u} = (\bar{u}^1, \dots, \bar{u}^n) \in C(\bar{I}) \text{ s.t. } \forall t \in \bar{I} \\ \qquad (u_t(t), v) + \mathfrak{b}_h(u(t), v) + \langle \bar{u}(t), v \rangle_{\Gamma_h} = \tilde{f}(t, v), \qquad \forall v \in \mathcal{V}, \\ \qquad\qquad (u(0), w) = (u_0, w), \qquad \forall w \in \mathcal{U}, \end{cases} \tag{10}$$

with $\mathfrak{b}_h(\cdot, \cdot)$ refering to (5) element-wise and

$$\langle \bar{u}(t), v \rangle_{\Gamma_h} := -\sum_{i=1}^{n} \bar{u}^i(t) b[v]_i,$$

where the jumps terms are $[v]_i = v(x_i^+) - v(x_i^-),\ \forall i = 1, \dots, n-1$ and $[v]_n = -v(x_n^-)$.

Selecting in this case

$$\mathcal{U}_h := \mathcal{P}^p(\Omega_h), \quad \mathcal{V}_h := \mathcal{P}^{p+\Delta p}(\Omega_h), \tag{11}$$

with $\Delta p \geq 1$, we obtain from (29) the following system of ODEs

$$\begin{cases} MU'(t) + KU(t) + R\bar{u}(t) = \tilde{F}(t),\ \forall t \in \bar{I}, \\ \qquad\qquad M_0 U(0) = \tilde{U}_0, \end{cases} \tag{12}$$

where R is the matrix corresponding to the interface contributions. Here, we are slightly abusing notation as matrices M and K in (12) are different from the ones in (8).

The ODE system in (12) is non-square and in order to symmetrize it we need to introduce the idea of optimal testing [10]. Given an inner product $(\cdot, \cdot)_{\mathcal{V}}$ on $\mathcal{V}$, we introduce the optimal test functions corresponding to u and $\bar{u}$ for a fixed $t \in \bar{I}$, respectively, as the solution of the following variational problems

$$\begin{cases} \text{Given } \delta u \in \mathcal{U} \text{ find } v_{\delta u} \in \mathcal{V} \text{ s.t} \\ (v_{\delta u}, \delta v)_{\mathcal{V}} = \mathfrak{b}_h(\delta u, \delta v),\ \forall \delta v \in \mathcal{V}, \end{cases} \qquad \begin{cases} \text{Given } \delta \bar{u} \in \mathbb{R}^n \text{ find } v_{\delta \bar{u}} \in \mathcal{V} \text{ s.t} \\ (v_{\delta \bar{u}}, \delta v)_{\mathcal{V}} = \langle \delta \bar{u}, \delta v \rangle_{\Gamma_h},\ \forall \delta v \in \mathcal{V}. \end{cases} \tag{13}$$

Discretizing (13) employing (11), we obtain that the optimal test functions for any $\delta u_h \in \mathcal{U}_h$ and $\delta \bar{u} \in \mathbb{R}^n$ are

$$v_{\delta u_h} = G^{-1} K \delta u_h, \quad v_{\delta \bar{u}} = G^{-1} R \delta \bar{u}, \tag{14}$$

where G is the Gram matrix corresponding to the inner product defined on $\mathcal{V}$.

Finally, the optimal test functions (13) lead to the following square system of ODEs

$$\begin{cases} K^T G^{-1} M U'(t) + K^T G^{-1} K U(t) + K^T G^{-1} R \bar{u}(t) = K^T G^{-1} \tilde{F}(t),\ \forall t \in \bar{I}, \\ R^T G^{-1} M U'(t) + R^T G^{-1} K U(t) + R^T G^{-1} R \bar{u}(t) = R^T G^{-1} \tilde{F}(t), \\ \qquad\qquad M_0 U(0) = \tilde{U}_0, \end{cases} \tag{15}$$

and statically condensing the interface variables we obtain the final system of ODEs

$$\begin{cases} K^T S_1 M U'(t) + K^T S_1 K U(t) = K^T S_1 \tilde{F}(t), \ \forall t \in \bar{I}, \\ M_0 U(0) = \tilde{U}_0, \end{cases} \tag{16}$$

where

$$S_1 = G^{-1} - G^{-1} R (R^T G^{-1} R)^{-1} R^T G^{-1} \tag{17}$$

and the matrix A we obtain in (1) is

$$A = (K^T S_1 M)^{-1} K^T S_1 K. \tag{18}$$

Here, matrices K, M and G are block diagonal but R is not; it is a more general sparse matrix. Therefore, matrix A in (18) involves computing the inverse of a large fully populated matrix which is not practical.

3.3. Practical DPG formulation

In order to overcome the problem with the inversion, we maintain the optimal test function $v_{\delta u}$ for the fields in (13) and we introduce new optimal test functions for the interface variables that are orthogonal to the mass matrix M:

$$\begin{cases} \text{Given } \delta\bar{u} \in \mathbb{R}^n \text{ find } v_{\delta\bar{u}} \in \mathcal{V} \text{ and } u \in \mathcal{U} \text{ s.t} \\ (v_{\delta\bar{u}}, \delta v)_{\mathcal{V}} - \mathfrak{b}_h(u, \delta v) = \langle \delta\bar{u}, \delta v \rangle_{\Gamma_h}, \ \forall \delta v \in \mathcal{V}. \\ (\delta u, v_{\delta\bar{u}}) = 0, \qquad \forall \delta u \in \mathcal{U}. \end{cases} \tag{19}$$

Here, we are augmenting space of optimal test functions corresponding to fields with particular test functions that are orthogonal to the mass matrix. Comparing to (13), we are essentially changing the basis but not the optimal test space. Discretizing (19) with (11) we obtain that $v_{\delta\bar{u}} = S_2^T R \delta\bar{u}$ where

$$S_2 = G^{-1} - G^{-1} M (K^T G^{-1} M)^{-1} K^T G^{-1}, \tag{20}$$

which leads to the following system of ODEs

$$\begin{cases} K^T G^{-1} M U'(t) + K^T G^{-1} K U(t) + K^T G^{-1} R \bar{u}(t) = K^T G^{-1} \tilde{F}(t), \ \forall t \in \bar{I}, \\ R^T S_2 K U(t) + R^T S_2 R \bar{u}(t) = R^T S_2 \tilde{F}(t), \\ M_0 U(0) = \tilde{U}_0, \end{cases} \tag{21}$$

and again, statically condensing the interface variables

$$\bar{u}(t) = (R^T S_2 R)^{-1} (R^T S_2 \tilde{F}(t) - R^T S_2 K U(t)), \tag{22}$$

we obtain the final system of ODEs

$$\begin{cases} K^T G^{-1} M U'(t) + K^T S_3 K U(t) = K^T S_3 \tilde{F}(t), \ \forall t \in \bar{I}, \\ M_0 U(0) = \tilde{U}_0, \end{cases} \tag{23}$$

where

$$S_3 = G^{-1} - G^{-1}R(R^T S_2 R)^{-1} R^T S_2, \tag{24}$$

and the matrix we obtain in (1) is

$$A = (K^T G^{-1} M)^{-1} K^T S_3 K. \tag{25}$$

Here, the inversion of matrix $K^T G^{-1} M$ can be computed locally. We will discuss in Section 4.2 how we can compute the exponential of (25) efficiently without assembling the full matrix A.

Remark 1. *Note that if we restrict methods (18) and (25) to the conforming case, i.e, selecting for $\mathcal{V}_h$ polynomials in $H^1_+(\Omega)$ with $\Delta p = 1$ then $R = 0$, M and K are square matrices and we recover matrix* (9).

3.4. Selection of the inner product

In the definition of the optimal test functions (13) and (19), we need to select an inner product in $\mathcal{V}$. We focus on two norms: the adjoint graph norm that is usually employed in DPG for the ultraweak variational setting

$$||v||^2_{\mathcal{V}} = \sum_{i=1}^{n} ||v||^2_{\Omega_i} + ||-bv_x + cv||^2_{\Omega_i}, \tag{26}$$

and also the following localizable adjoint norm motivated by [32]

$$||v||^2_{\mathcal{V}} = \sum_{i=1}^{n} ||-bv_x + cv||^2_{\Omega_i} + b|v(x_i^-)|^2, \tag{27}$$

where $||\cdot||_{\Omega_i}$ denotes the L^2-norm over each element Ω_i. In higher space dimensions, (27) corresponds to adding the outflow contribution as in [8].

In the case of pure advection ($c = 0$), we select norm (27) because the adjoint graph norm (26) leads a singular $K^T G^{-1} M$ matrix in (25) (see Appendix A).

4. Semidiscretization in time

We now define a mesh I_τ of I

$$0 = t_0 < t_1 < \ldots < t_{m-1} < t_m = 1,$$

where $I_k = (t_{k-1}, t_k)$ and $\tau_k = t_k - t_{k-1}$, $\forall\, k = 1, \ldots, m$ and $\tau = \max_{1 \le k \le m} \tau_k$. We denote by Γ_τ the mesh skeleton in time. In this section, we include a brief summary of the DPG time-marching scheme introduced in [32]. We then discuss the efficiency of computing the φ-function of matrix A in (25).

4.1. DPG time-marching scheme

We focus on system (1) being

$$A = (K^T G^{-1} M)^{-1} K^T S_3 K, \;\; F(t) = (K^T G^{-1} M)^{-1} K^T S_3 \tilde{F}(t), \;\; U_0 = M_0^{-1} \tilde{U}_0, \tag{28}$$

from the DPG semidiscretization introduced Section 3.3. We denote by $\mathbb{U} := L^2(I, \mathbb{R}^s)$ and $\mathbb{V} := H^1(I_\tau, \mathbb{R}^s)$ and we consider the following broken ultraweak variational formulation in time

$$\begin{cases} \text{Find } U \in \mathbb{U} \text{ and } \hat{U} = (\hat{U}^1, \ldots, \hat{U}^m) \in \mathbb{R}^{s \times m} \text{ s.t.} \\ B_\tau(U, V) + \langle \hat{U}, V \rangle_{\Gamma_\tau} = \displaystyle\int_I (F(t), V) dt + U_0 V(0), \;\; \forall V \in \mathbb{V}, \end{cases} \tag{29}$$

where

$$B_\tau(U, V) + \langle \hat{U}, V \rangle_{\Gamma_\tau} := \sum_{k=1}^{m} \int_{I_k} (U, -V' + A^T V) dt - (\hat{U}^k, [V]_k).$$

Here, $(\cdot, \cdot)$ denotes the usual dot product in $\mathbb{R}^s$ and $[V]_k = V(t_k^+) - V(t_k^-), \; \forall k = 1, \ldots, m-1$ and $[V]_m = -V(t_m^-)$.

Similar to (13), we define the optimal test functions in time as

$$\begin{cases} \text{Given } \delta U \in \mathbb{U} \text{ find } V_{\delta u} \in \mathbb{V} \text{ s.t} \\ (V_{\delta u}, \delta V)_{\mathbb{V}} = B_\tau(\delta U, \delta V), \; \forall \delta V \in \mathbb{V}, \end{cases} \qquad \begin{cases} \text{Given } \delta \hat{U} \in \mathbb{R}^{s \times m} \text{ find } V_{\delta \hat{U}} \in \mathbb{V} \text{ s.t} \\ (V_{\delta \hat{U}}, \delta V)_{\mathbb{V}} = \langle \delta \hat{U}, \delta V \rangle_{\Gamma_h}, \; \forall \delta V \in \mathbb{V}, \end{cases} \tag{30}$$

where the inner product is

$$||V||_{\mathbb{V}}^2 = \sum_{k=1}^{m} || - V' + A^T V||_{I_k}^2 + |V(t_k^-)|^2, \tag{31}$$

where $|| \cdot ||_{I_k}$ denotes the L^2-norm over each time interval I_k. In this case, as (30) is essentially a 1D problem, we compute the optimal test functions analytically. Therefore, approximating the field variables with piecewise polynomials of order q, i.e.,

$$U(t)_{|_{I_k}} \approx U_\tau^k(t) := \sum_{l=0}^{q} U_{\tau,l}^k \left(\frac{t - t_{k-1}}{\tau_k} \right)^l, \; \forall k = 1, \ldots, m, \tag{32}$$

we obtain the following optimal test functions defined recursively at each time interval $\forall k = 1, \ldots, m$ as

$$\begin{cases} \hat{V}^k(A^T, t) = e^{A^T (t - t_k)}, \\ V_r^k(A^T, t) = \left(A^T\right)^{-1} \left(\left(\dfrac{t - t_{k-1}}{\tau_k} \right)^r I_s + \dfrac{r}{\tau_k} V_{r-1}^k(A^T, t) - \hat{V}^k(A^T, t) \right), \;\; \forall r = 0, \ldots, q, \end{cases} \tag{33}$$

where I_s denotes the identity matrix of order s, $\hat{V}^k$ are the optimal test functions corresponding to the trace variables $\hat{U}^k$ and V_r^k are the optimal test functions corresponding to

the fields. We know from [32] that functions (33) satisfy the adjoint equation and that they decouple the trace variables from the fields obtaining the final time-stepping scheme

$$\begin{cases} \hat{U}^k = \hat{V}(A, t_{k-1})\hat{U}^{k-1} + \displaystyle\int_{I_k} \hat{V}(A,t)F(t)dt, \\ \displaystyle\sum_{l=0}^{q} U_{\tau,l}^k \int_{I_k} \left(\frac{t-t_{k-1}}{\tau_k}\right)^{l+r} dt = V_r^k(A, t_{k-1})\hat{U}^{k-1} + \int_{I_k} V_r^k(A,t)F(t)dt, \ \forall r = 0, \ldots, q, \end{cases} \tag{34}$$

where $\hat{U}^0 = U_0$.

Figure 1 illustrates a single space-time element employing quadratic polynomials for space discretization and piecewise linear functions for the time-marching scheme. Here, we have space-time field variables, traces in time that depend upon space and traces in space that depend upon time.

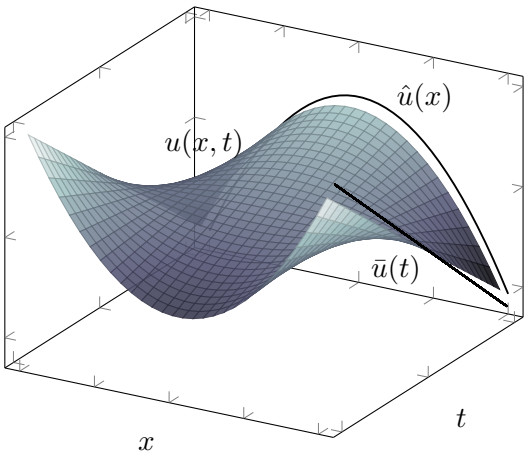

Figure 1: Space-time element with quadratic polynomials in space and linear polynomials in time. We denote here by $u(x,t)$ the field variables, $\hat{u}(x)$ the trace variables in time that depend upon space and $\bar{u}(t)$ the interface variables in space that depend upon time.

Remark 2. *In practice, we do not compute explicitly the traces in space (22). Their influence is implicit in the matrix A. In order to obtain an explicit system of equations to compute $\bar{u}$, we can consider a broken variational formulation in time directly in system (21). In this case, additionally to (33), we have optimal test functions corresponding to $\bar{u}$ (see Appendix B).*

4.2. Computing the exponential

Time-marching scheme (34) involves computing exponential-related functions of matrix A in (25). In [32], we proved that the optimal test functions in (33) can be expressed in

terms of the so-called φ-functions usually employed in exponential time integrators

$$\begin{cases} \varphi_0(z) = e^z, \\ \varphi_q(z) = \displaystyle\int_0^1 e^{(1-\theta)z} \frac{\theta^{q-1}}{(q-1)!} d\theta, \ \forall q \geq 1, \end{cases} \tag{35}$$

which satisfy the following recurrence formula

$$\varphi_{q+1}(z) = \frac{1}{z}\left(\varphi_q(z) - \frac{1}{q!}\right). \tag{36}$$

For example, the lowest order ($r = 0$) case in (34) reads

$$\begin{cases} \hat{U}^k = \hat{U}^{k-1} + \tau_k \varphi_1(-\tau_k A)(F(t_{k-1}) - A\hat{U}^{k-1}), \\ U^k_{\tau,0} = \varphi_1(-\tau_k A)\hat{U}^{k-1} + \tau_k \varphi_2(-\tau_k A)F(t_{k-1}). \end{cases} \tag{37}$$

Here, we obtain the classical Exponential Euler method for the trace variables.

There exists a wide variety of software to approximate the action of φ-functions over vectors [4, 29, 33]. We employ the routine introduced by Al-Mohy et. al. in [1] which is based in the following result

Theorem 1. *Let $A \in \mathbb{R}^{s\times s}$, $W = [w_1, \ldots, w_q] \in \mathbb{R}^{s\times q}$, and*

$$\tilde{A} = \begin{bmatrix} A & W \\ 0 & J \end{bmatrix} \in \mathbb{R}^{(s+q)\times(s+q)}, \quad J = \begin{bmatrix} 0 & I_{q-1} \\ 0 & 0 \end{bmatrix} \in \mathbb{R}^{q\times q};$$

it holds that

$$e^{\tilde{A}} b_j(1:s) = \sum_{l=1}^{j} \varphi_l(A) w_{j-l+1}, \ \ \forall j = 1, \ldots, q, \tag{38}$$

b_j being the j-vector in the canonical basis in $\mathbb{R}^s$.

Proof. See [1] Theorem 2.1. □

In (38), notation $(1 : s)$ denotes the first s entries of vector $e^{\tilde{A}} b_j$. Therefore, the computation of linear combinations of actions of φ-functions over vectors as in (37), is simplified to the action of a single exponential of a slightly larger matrix $\tilde{A}$.

The strategy in [1] to compute the action of the exponential is based on the squaring and scaling algorithm

$$e^{\tilde{A}} b_j \approx \left(T_m\left(\frac{1}{\sigma}\tilde{A}\right)\right)^{\sigma} b_j$$

being T_m a truncated Taylor series. The values of m and σ are selected based on the 1-norm of matrix $\tilde{A}$ and the algorithm performs matrix-vector multiplications.

In the method presented in Section 3.3, matrix A (25), involves matrices (20) and (24). In (11), we denote by $s := \dim(\mathcal{U}_h)$ and $r := \dim(\mathcal{V}_h)$, where $r \gg s$ and we have that

$$M, K \in \mathbb{R}^{r\times s}, \;\; G \in \mathbb{R}^{r\times r}, \;\; R \in \mathbb{R}^{r\times n},$$

n being the number of interface variables in space. In (20), matrix $S_2 \in \mathbb{R}^{r\times r}$ is given by a product of block diagonal matrices so it can be computed element-wise. Then, we can rewrite the final matrix of the system as

$$A = \underbrace{(K^T G^{-1} M)^{-1} K^T G^{-1} K}_{A_1} - \underbrace{(K^T G^{-1} M)^{-1} K^T G^{-1} R}_{A_2} \underbrace{(R^T S_2 R)^{-1}}_{A_3} \underbrace{R^T S_2 K}_{A_4}, \tag{39}$$

where

- $A_1 \in \mathbb{R}^{s\times s}$ is block diagonal.
- $A_2 \in \mathbb{R}^{s\times n}$ and $A_4 \in \mathbb{R}^{n\times s}$ are dense but thin.
- $A_3 \in \mathbb{R}^{n\times n}$ is dense but small.

On the other hand, we know that

$$||\tilde{A}||_1 = \begin{cases} \max(||A||_1, ||W||_1), & \text{if } q = 1, \\ \max(||A||_1, ||W||_1 + 1), & \text{if } q \geq 2, \end{cases}$$

and from the properties of the 1-norm we know

$$||A||_1 \leq ||A_1||_1 + ||A_2||_1 ||A_3||_1 ||A_4||_1,$$

where $||A_1||_1$ can be computed block-wise.

In conclusion, we can perform matrix-vector products and estimation of the norm of $\tilde{A}$ needed to compute the right-hand-side of (34), in terms of the four matrices defined in (39). In other words, we can compute the actions of φ-functions of A without assembling the matrix A itself.

Remark 3. *We select monomials in the time discretization (32) for the field variables because the relation between the corresponding optimal test functions and the φ-functions is simpler from the definition in (35). However, other basis functions in time can be considered.*

5. Consistency with steady-state solutions

In this section, we study the consistency of our time-marching scheme with steady-state solutions. In other words, if we consider an ultraweak DPG approximation of the steady-state advection-reaction equation, we shall recover the same solution if we solve system (1) with the steady-state data (time-independent source and initial condition).

We first consider the steady-state problem

$$\begin{cases} bu'(x) + cu(x) = f(x), & \text{in } \Omega, \\ u(0) = g. \end{cases} \tag{40}$$

The ultraweak DPG solution $\{U_h, \bar{u}_h\}$ of (40) reads

$$\begin{bmatrix} K^T G^{-1} K & K^T G^{-1} R \\ R^T G^{-1} K & R^T G^{-1} R \end{bmatrix} \begin{bmatrix} U_h \\ \bar{u}_h \end{bmatrix} = \begin{bmatrix} K^T G^{-1} \tilde{F}_h \\ R^T G^{-1} \tilde{F}_h \end{bmatrix}, \tag{41}$$

and, therefore, $U_h = (K^T S_1 K)^{-1} K^T S_1 \tilde{F}_h$ with S_1 defined in (17). Now, we solve the following system of ODEs with the DPG time-marching scheme (34)

$$\begin{cases} U'(t) + AU(t) = F_h, \ \forall t \in \bar{I}, \\ U(0) = U_h, \end{cases} \tag{42}$$

where $A = (K^T S_1 M)^{-1} K^T S_1 K$ and S_1 are defined as in Section 3.2 and $F_h := (K^T S_1 M)^{-1} K^T S_1 \tilde{F}_h$. Note that

$$F_h = (K^T S_1 M)^{-1} K^T S_1 \tilde{F}_h = (K^T S_1 M)^{-1} K^T S_1 K U_h = A U_h.$$

We focus on (34) for a single time ($m = T = 1$) step to verify that we recover the DPG solution U_h. Here, F_h is time-independent, so for the first equation of (34) we obtain

$$\begin{aligned} \hat{U}^1 &= \hat{V}(A,0) U_h + \int_0^1 \hat{v}(A,t) dt F_h = e^{-A} U_h + \int_0^1 e^{A(t-1)} dt F_h \\ &= e^{-A} U_h + A^{-1}(I - e^{-A}) F_h = e^{-A} U_h + A^{-1}(I - e^{-A}) A U_h = U_h; \end{aligned}$$

therefore, we have $\hat{U}^1 = U_h$. Similarly, for the field variables

$$\sum_{l=0}^{q} \frac{1}{l+r+1} U_{\tau,l}^1 = V_r^1(A,0) U_h + \int_0^1 V_r^1(A,t) dt F_h, \ \forall r = 0, \ldots, q,$$

and we know from [32] the following relations

$$V_r^1(A,0) = \sum_{j=0}^{r} \frac{r!}{j!} (-1)^{r-j} \varphi_{r-j+1}(-A), \quad \int_0^1 V_r^1(A,t) dt = \sum_{j=0}^{r} \frac{r!}{j!} (-1)^{r-j} \varphi_{r-j+2}(-A).$$

Therefore, from $F_h = A U_h$ we have that

$$\sum_{l=0}^{q} \frac{1}{l+r+1} U_{\tau,l}^1 = \sum_{j=0}^{r} \frac{r!}{j!} (-1)^{r-j} \left(\varphi_{r-j+1}(-A) + \varphi_{r-j+2}(-A) A \right) U_h, \ \forall r = 0, \ldots, q,$$

and from recurrence relation (36)

$$\sum_{l=0}^{q} \frac{1}{l+r+1} U_{\tau,l}^1 = \sum_{j=0}^{r} \frac{r!}{j!} (-1)^{r-j} \frac{1}{(r-j+1)!} U_h, \ \forall r = 0, \ldots, q.$$

We observe that

$$\sum_{j=0}^{r} \frac{r!}{j!}(-1)^{r-j}\frac{1}{(r-j+1)!} = \frac{1}{r+1}\sum_{j=0}^{r}\binom{r+1}{j}(-1)^{r-j} = \frac{1}{r+1}\left((-1)^r + \sum_{j=1}^{r}\binom{r+1}{j}(-1)^{r-j}\right)$$
$$= \frac{1}{r+1}\left((-1)^r + \sum_{j=1}^{r}\left[\binom{r}{j} + \binom{r}{j-1}\right](-1)^{r-j}\right)$$
$$= \frac{1}{r+1}\left((-1)^r + \sum_{j=1}^{r}\binom{r}{j}(-1)^{r-1} + \sum_{j=0}^{r-1}\binom{r}{j}(-1)^{r-j+1}\right)$$
$$= \frac{1}{r+1}\left((-1)^r + 1 + (-1)^{r+1}\right) = \frac{1}{r+1},$$

and finally,

$$\sum_{l=0}^{q}\frac{1}{l+r+1}U_{\tau,l}^1 = \frac{1}{r+1}U_h,\ \forall r = 0,\dots,q,$$

which implies that $U_{\tau,0}^1 = U_h$ and $U_{\tau,l}^1 = 0, \forall l = 1,\dots,q$. In conclusion, extending this reasoning to an arbitrary number of time steps we have that

$$\hat{U}^k = U_{\tau,0}^k = U_h,\ \ U_{\tau,l}^k = 0,\ \ \forall l = 1,\dots,q,\ \ \forall k = 1,\dots,m,$$

i.e., we recover the DPG solution from the steady-state problem for both trace and field variables in time.

Remark 4. *In order to recover the steady-state DPG solution from the practical method defined in Section 3.3, we would need to consider a DPG method to discretize (40) with the particular optimal test functions defined in (19).*

6. Numerical results

In this section, we show the performance of the semidiscretizations presented in Section 3 together with the DPG time-marching scheme from Section 4.1. We first mention some observations from computations:

- The practical DPG method presented in Section 3.3 delivers the same solution as the classical DPG discretization from Section 3.2 for any problem.
- For convection-reaction problems we do not observe any difference between employing the localizable norm (27) or the adjoint graph norm (26). For pure convection problems, we consider norm (27) to ensure that we obtain non-singular matrices.
- In pure convection problems, the three discretizations in Section 3 deliver the same solution. This is consistent with the fact that the space in 3.1 corresponds to the optimal test space of the DPG method for this particular case.

- We show in Section 6.3 that for convection-reaction problems with a large reaction coefficient, the DPG method delivers an optimal solution whereas with the PG method we lose the optimal convergence rates for the lowest-order polynomial degrees.

Therefore, in all examples but 6.3 in this section we employ the practical DPG method from Section 3.3 with the localizable norm (27) and $\Delta p = 1$.

We denote by $u_{\tau h}(x,t)$ the final approximation for the space-time field variables which are the coefficients obtained from the second equation of (34) multiplied by the tensor products of shape functions in space and time. We measure the error of the field variables in the $L^2(I;L^2(\Omega))$ norm, i.e.,

$$\mathcal{E} := \left(\int_I ||u(x,t) - u_{\tau h}(x,t)||^2_{L^2(\Omega)} dt \right)^{1/2}. \tag{43}$$

Similarly, we denote by $\hat{u}_h(x) = (\hat{u}_h^1(x), \ldots, \hat{u}_h^m(x))$ the approximation for the traces we obtain from the coefficients of the first equation of (34) times the shape functions in space. We will consider the following two norms for the error in the trace variables

$$\hat{\mathcal{E}}_1 := \left(\sum_{k=1}^{m} ||u(x,t_k) - \hat{u}_h^k(x)||^2_{L^2(\Omega)} \right)^{1/2}, \tag{44}$$

$$\hat{\mathcal{E}}_2 := \max_{1\leq k\leq m} ||u(x,t_k) - \hat{u}_h^k(x)||_{L^2(\Omega)}. \tag{45}$$

In general, for the convergence in space, we fix a fine high-order grid in time and we measure error (43) while we refine the mesh in space for different polynomial orders, and vice versa for the convergence in time. We selected several problems for which we know the analytical solution.

6.1. Smooth solution

Here, we compute the convergence rates in both space and time for smooth data. We consider $T = 1$, $b = 1$, $c = 0$ and the data according to the following manufactured solution

$$u(x,t) = \cos(\pi t)\sin(\pi x). \tag{46}$$

Figures 2 and 3 show the approximation of field and trace variables, respectively, for different polynomial orders in both space and time. We selected 2^{4-p} elements in space and 2^{4-q} time steps.

Figure 4 displays the convergence in both space and time for the field variables. We observe optimal L^2-convergence rates in both cases: $\mathcal{O}(\tau^{q+1})$ and $\mathcal{O}(h^{p+1})$.

Figure 5 shows the convergence in space and time for the trace variables in both norms (44) and (45). Here, the equation to compute the traces in (34) is equivalent to classical exponential integrators employing exponential quadrature rules. We know from the literature that these methods are optimal in the maximum norm (45) for sufficiently smooth data.

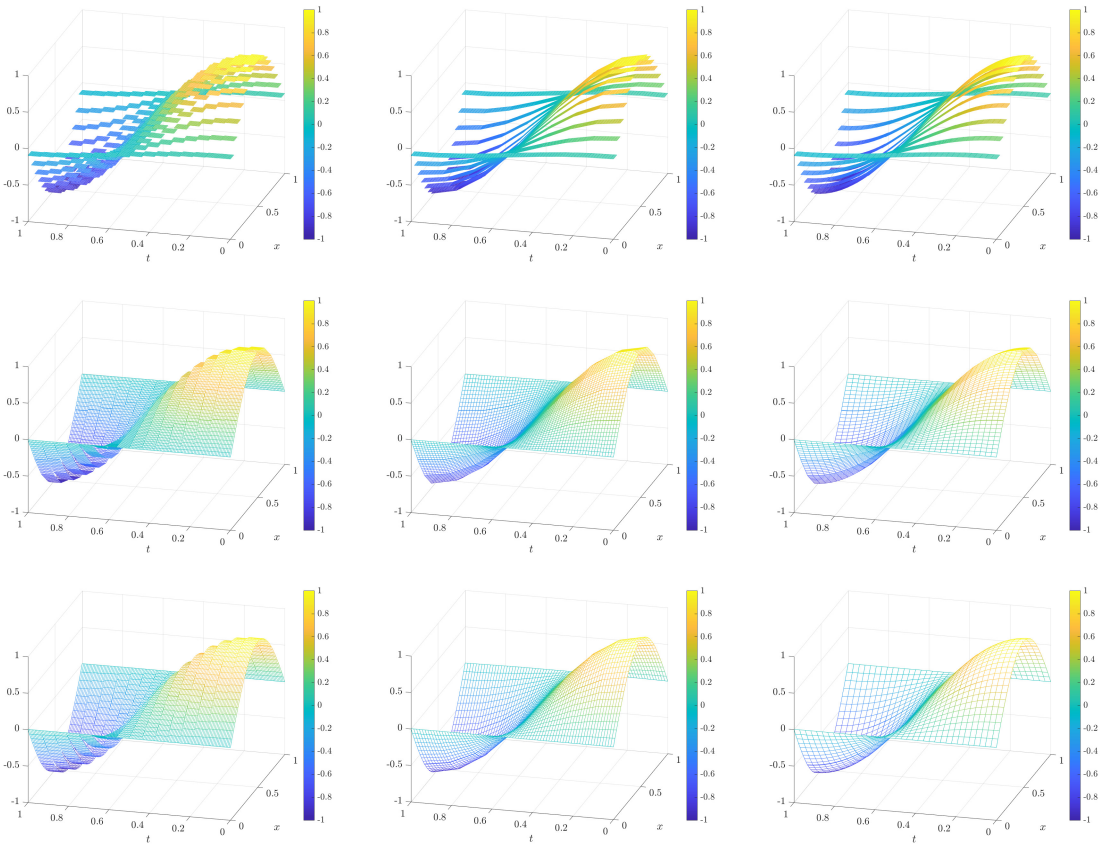

Figure 2: Approximation of fields for (46) with $p = 0, 1, 2$ (rows) and $q = 0, 1, 2$ (columns) for different element sizes.

Therefore, in the time convergence we observe optimal convergence rates in the maximum norm $\hat{\mathcal{E}}_2$ ($\mathcal{O}(\tau^{q+1})$) and suboptimal in the discrete L^2-norm $\hat{\mathcal{E}}_1$ ($\mathcal{O}(\tau^{q+1/2})$). Note that for $q = 2$ we have superconvergence in this particular example. On the other hand, we obtain optimal rates $\mathcal{O}(h^{p+1})$ in space for both norms.

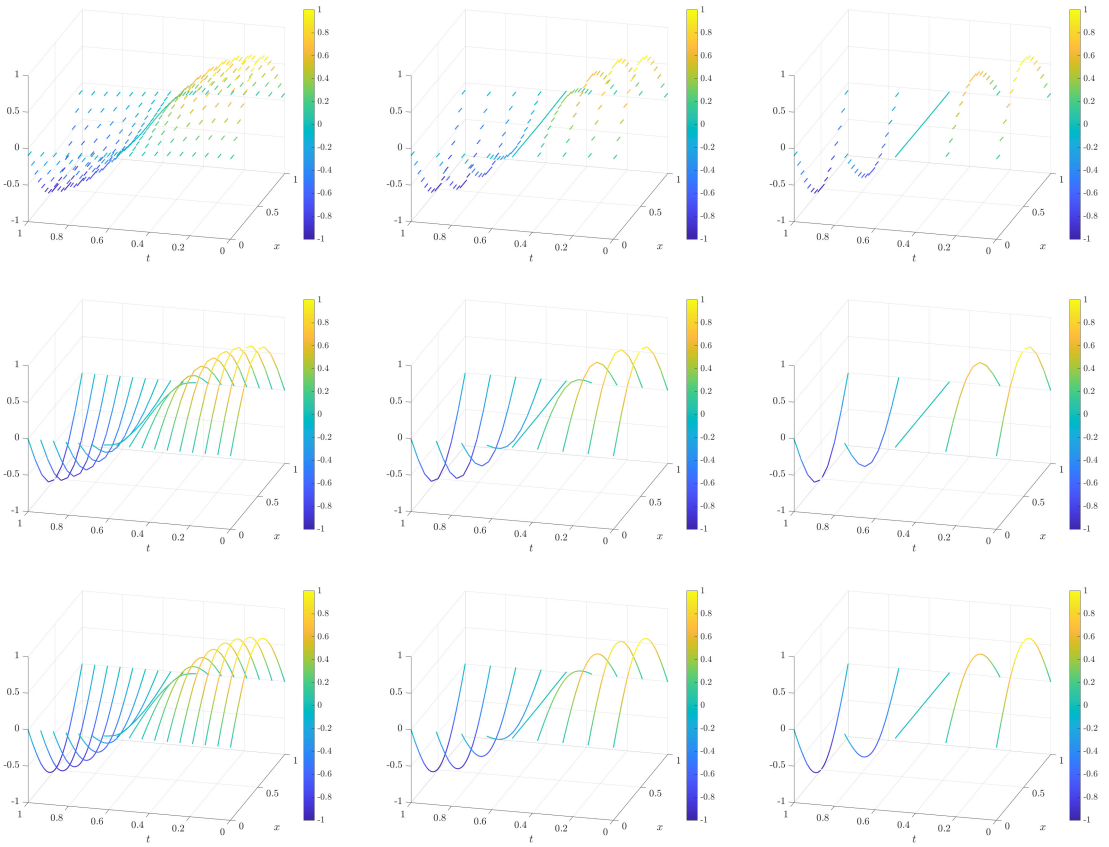

Figure 3: Approximation of traces for (46) with $p = 0, 1, 2$ (rows) and $q = 0, 1, 2$ (columns) for different element sizes.

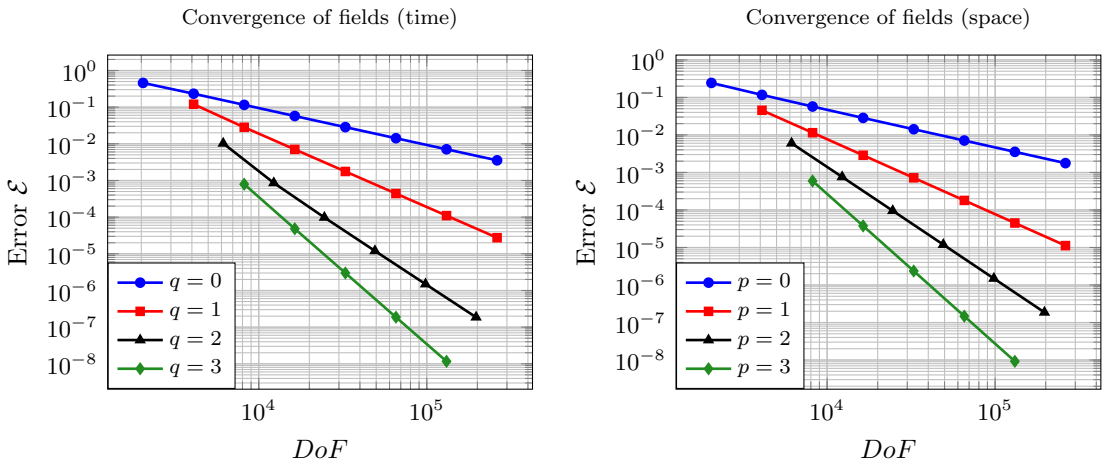

Figure 4: Convergence of field variables in time with $q = 0, 1, 2, 3$ (left) and space with $p = 0, 1, 2, 3$ (right) for the smooth manufactured solution (46).

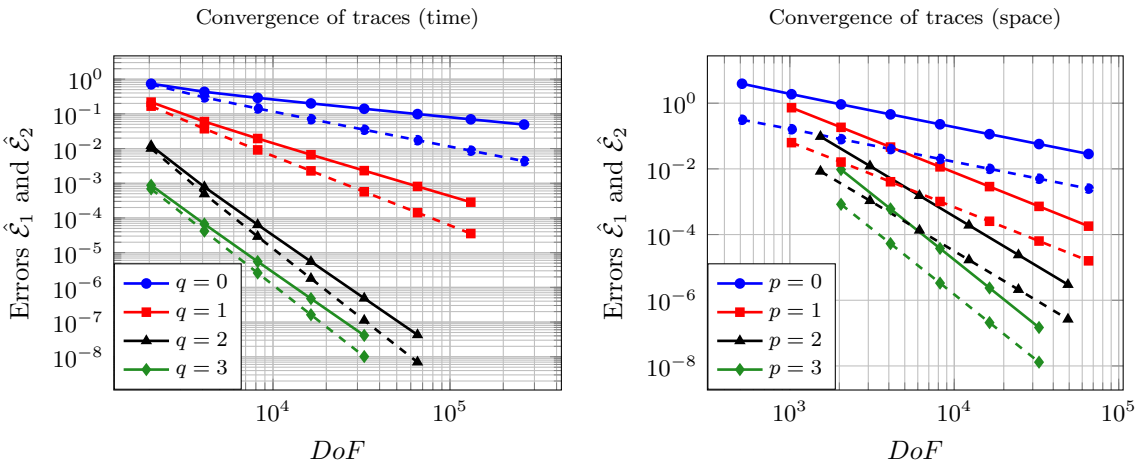

Figure 5: Convergence of trace variables in time with $q = 0, 1, 2, 3$ (left) and space with $p = 0, 1, 2, 3$ (right) for the smooth manufactured solution (46). Solid lines refer to error $\hat{\mathcal{E}}_1$ and dashed lines to error $\hat{\mathcal{E}}_2$.

6.2. Smooth solution with time dependent inflow data

We now consider $T = 3/4$, $b = 1$, $c = 1$ and the data according to the following manufactured solution

$$u(x,t) = \frac{\sin(\pi(x-t))^2}{1 - t\sin(\pi(x-t))^2}, \tag{47}$$

where the inflow condition is time dependent.

Figure 6 shows the fields and traces with $p = q = 2$ and 2^4 elements in space and 2^4 time steps. In Figure 7 we show the converge of the fields in time and space. We observe optimal convergence rates of $\mathcal{O}(\tau^{q+1})$ and $\mathcal{O}(h^{p+1})$, respectively. Finally, Figure 8 displays the convergence in the trace variables. As in the previous example, we obtain optimal convergence rates $\mathcal{O}(h^{p+1})$ in space for both norms and in time, we observe $\mathcal{O}(\tau^{q+1})$ for norm $\hat{\mathcal{E}}_2$ and $\mathcal{O}(\tau^{q+1/2})$ for norm $\hat{\mathcal{E}}_1$.

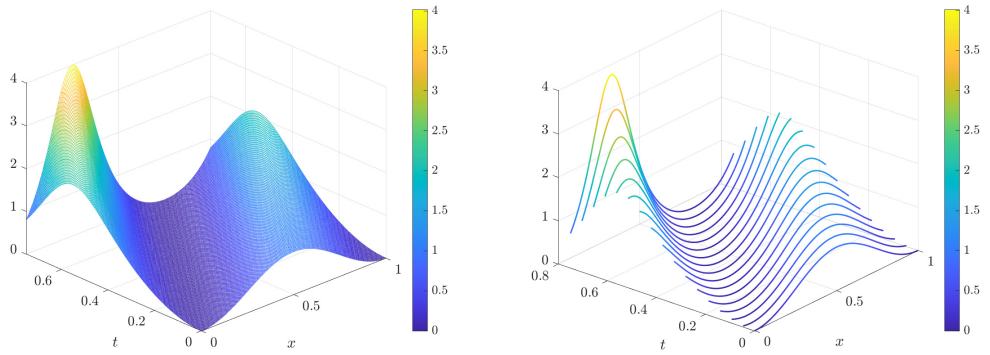

Figure 6: Approximation of fields and traces for solution (47) with $p = q = 2$.

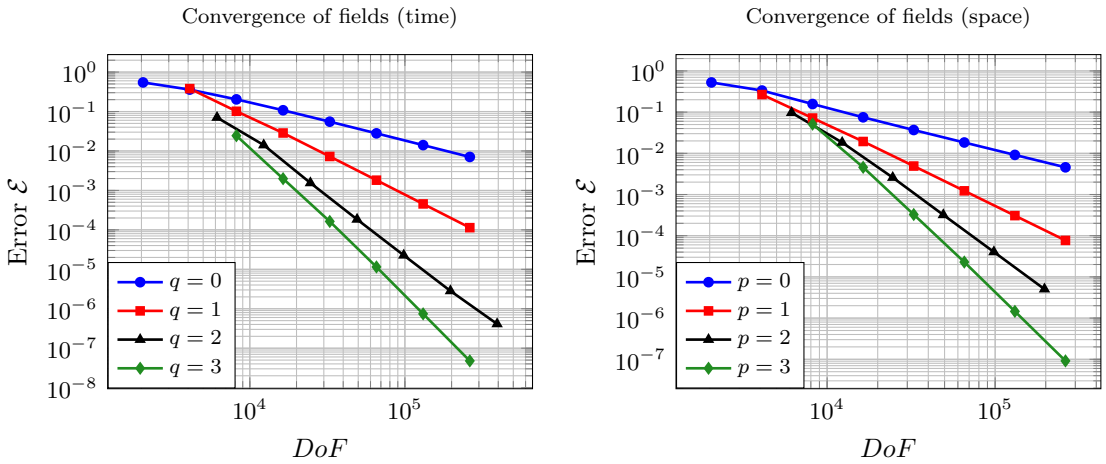

Figure 7: Convergence of field variables in time with $q = 0, 1, 2, 3$ (left) and space with $p = 0, 1, 2, 3$ (right) solution (47).

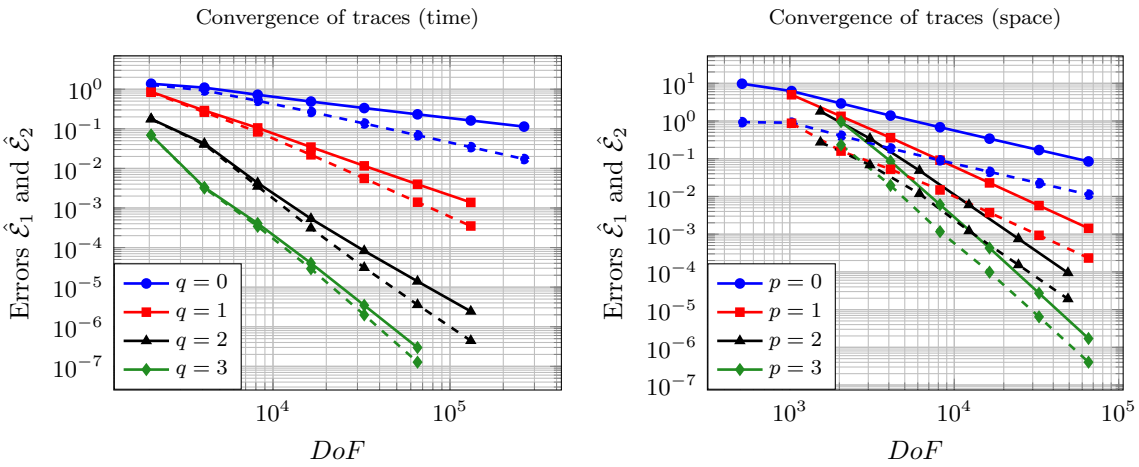

Figure 8: Convergence of trace variables in time with $q = 0, 1, 2, 3$ (left) and space with $p = 0, 1, 2, 3$ (right) for solution (47). Solid lines refer to error $\hat{\mathcal{E}}_1$ and dashed lines to error $\hat{\mathcal{E}}_2$.

6.3. Smooth solution with large reaction term

We now consider the same example as in Section 6.1 but with $T = 1$, $b = 1$, $c = 10^4$ and the data according to the same manufactured solution

$$u(x, t) = \cos(\pi t) \sin(\pi x). \tag{48}$$

Figure 9 displays the approximation of traces at $t = 0.25$ employing in space the PG method and the DPG method with $\Delta p = 2$ for different polynomial orders and 2^{4-p} elements. We see that for $p = 2$ the difference is minimal, but for $p = 0$ and $p = 1$ we observe that DPG method delivers the L^2-projection of the analytical solution (as expected) whereas the PG method does not. This phenomenon is reflected in the convergence plots in Figures 10 and 11 where we observe optimal convergence rates for the DPG method as in the previous examples. However, for the PG method we lose one order for $p = 1$ in both fields and traces.

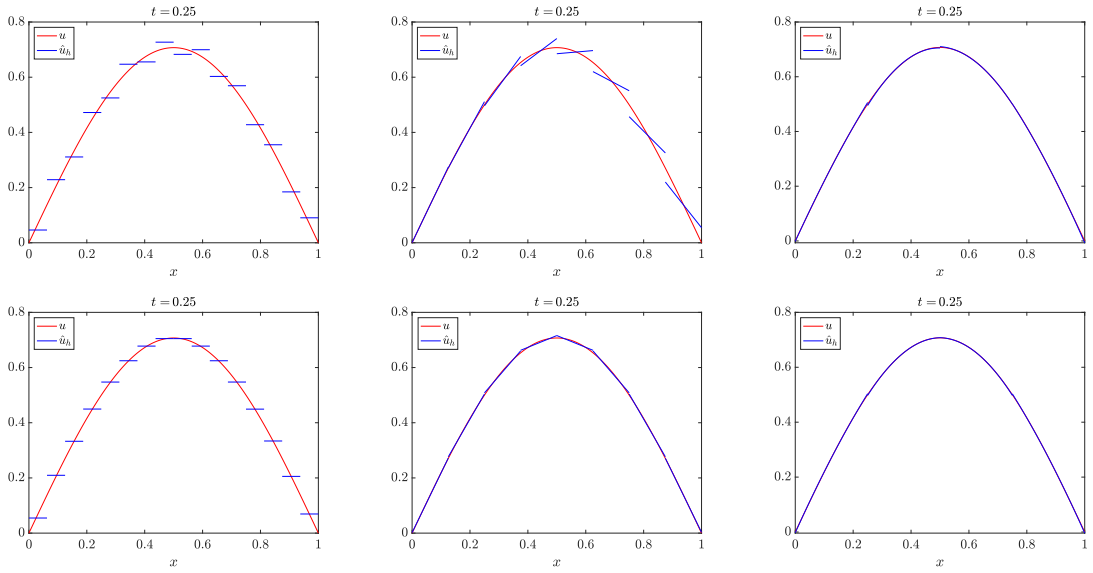

Figure 9: Approximation at $t = 0.25$ of solution (48) with large reaction coefficient employing PG method in space (top row) and DPG method (bottom row) for $p = 0, 1, 2$.

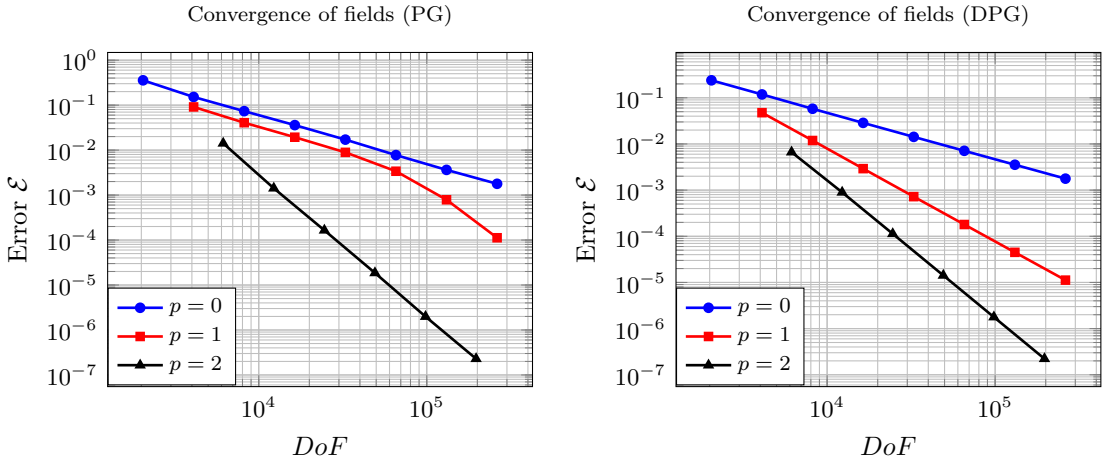

Figure 10: Convergence of field variables in space employing PG method (left) and the DPG method (right) with $p = 0, 1, 2$ for solution (48) with large reaction coefficient.

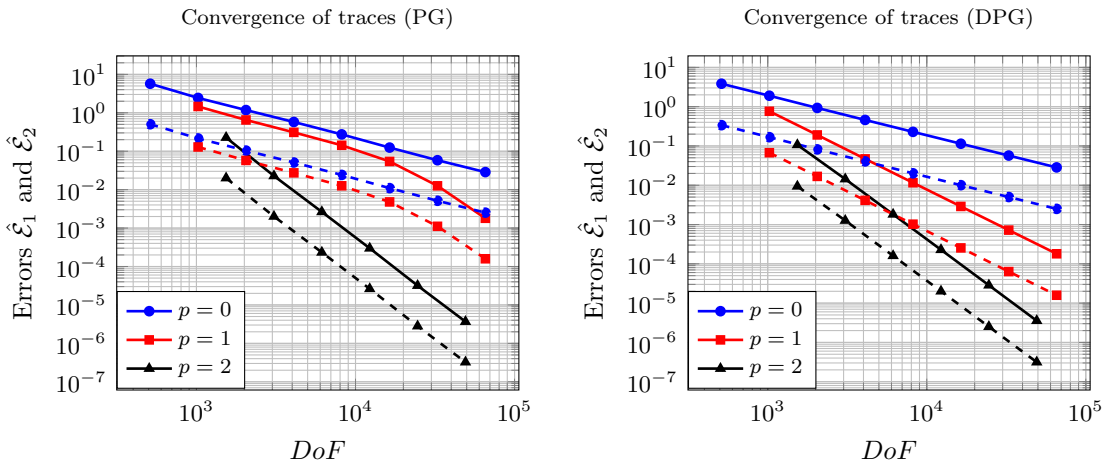

Figure 11: Convergence of traces in space employing PG method (left) and the DPG method (right) with $p = 0, 1, 2$ for solution (48) with large reaction coefficient. Solid lines refer to error $\hat{\mathcal{E}}_1$ and dashed lines to error $\hat{\mathcal{E}}_2$.

6.4. Continuous non-smooth solution

We consider now problem (2) with $T = 1$, $b = 1$, $c = 0$, $f = 0$ and a "hat" function as an initial condition

$$u_0(x) = \begin{cases} \dfrac{x - 0.25}{0.25}, & x \in (0.25, 0.5], \\ \dfrac{0.75 - x}{0.25}, & x \in (0.5, 0.75), \\ 0, & \text{elsewhere.} \end{cases} \tag{49}$$

We know that in this case the analytical solution is $u(x, t) = u_0(x - t)$.

Figure 12 shows approximation of fields and traces for $p = q = 1$ and we can conclude that the time marching scheme captures the corners of the solution without oscillations. For the field variables we observe in Figure 13 a convergence of order 1 for $p = 0$ in both space and time whereas for $p = 1$ we obtain a rate of $1 + 1/2$ in time and $1 + 1/5$ in space. Finally, in Figure 14 we have the same convergence rates in space as for the field variables.

Note that in this example, as $f = 0$, we have that the classical exponential integrator (first equation in (34)) delivers simply the exact solution at each time step, i.e., there is no time approximation. Therefore, the error in time for the trace variables in this example is simply zero. The same applies in the next example.

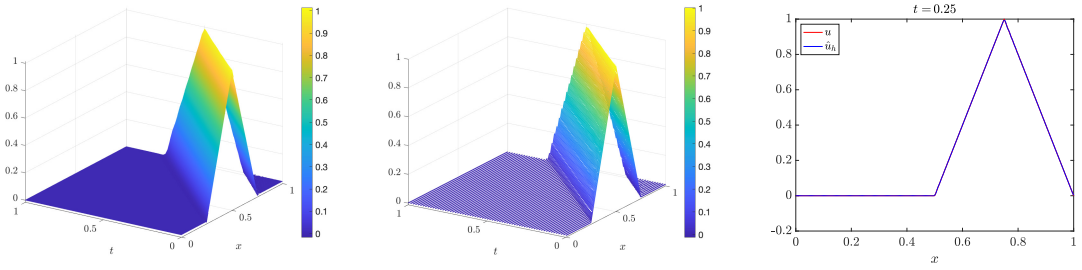

Figure 12: Approximation of fields and traces for (49) with $p = q = 1$.

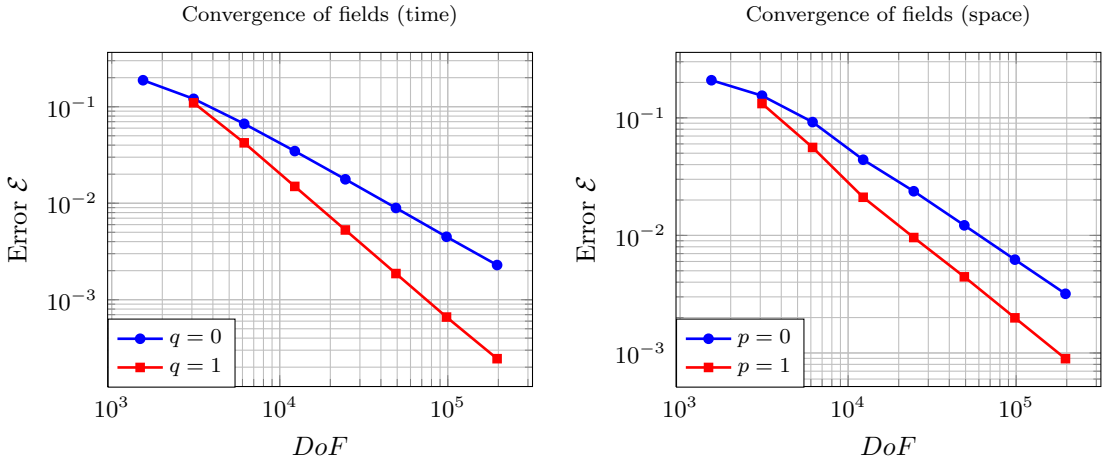

Figure 13: Convergence of fields variables in time (left) with $q = 0, 1$ and space (right) with $p = 0, 1$ for (49).

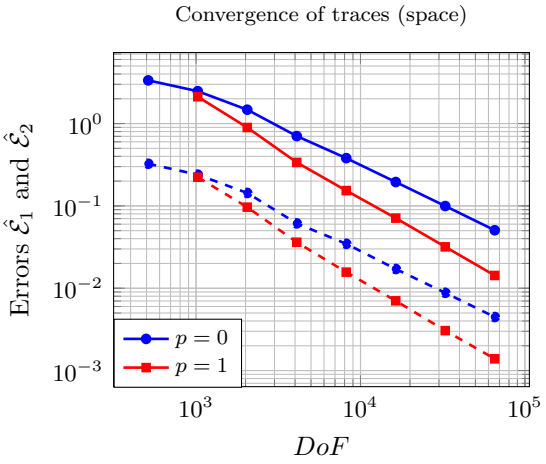

Figure 14: Convergence of trace variables in space with $p = 0, 1$ for solution (49). Solid lines refer to error $\hat{\mathcal{E}}_1$ and dashed lines to error $\hat{\mathcal{E}}_2$.

6.5. Discontinuous solution

We consider the same setting as in Section 6.4 but with a discontinuous initial condition

$$u_0(x) = \begin{cases} x^2, & x < 0.5, \\ -x^2, & x \geq 0.5. \end{cases} \tag{50}$$

In this example, in Figures 15 and 16 we observe for fields a convergence rate of 0.5 for $q = 0, 1, 2$ in time and rates of $0.3, 0.35, 0.38$ for $p = 0, 1, 2$ in space, respectively.

Figure 18 displays the traces and fields for 2^7 elements in space and 2^6 time steps with $q = 0$ and $p = 2$. Finally, in Figure 17 we display different snapshots of traces and fields for $q = 0$ and $p = 2$. in the first two rows we show the solutions of traces at $t = 0.25$ and fields at $t = 0.25 + \tau/2$, respectively, for a fine grid in time and different meshes in space. In the last row, we show the solution of fields at $t = 0.25 + \tau/2$ for a fixed fine mesh in space and different time step sizes. The solutions for traces in this case correspond to the classical exponential Euler method. We conclude that the solution in the element interior, i.e., the DPG solution in time, is less oscillatory that the classical exponential Euler method and it captures the space-time discontinuity.

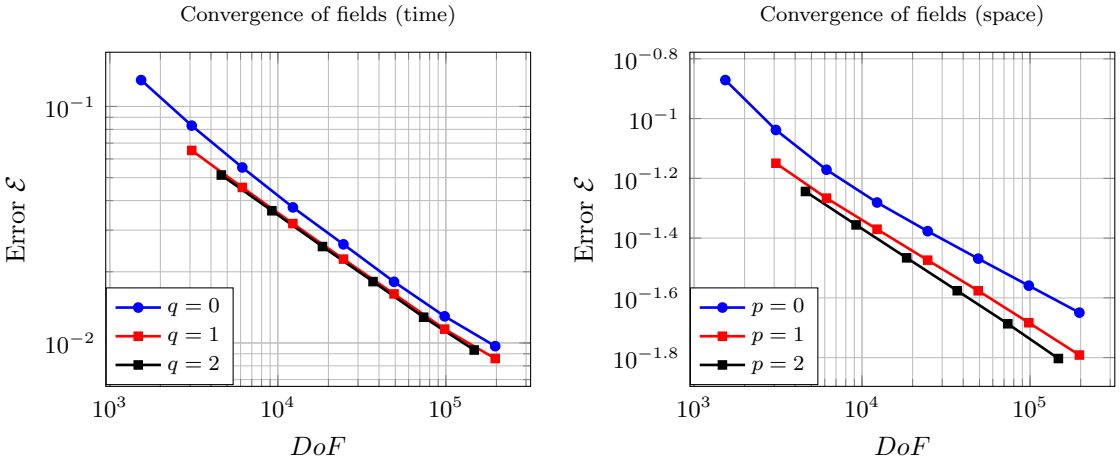

Figure 15: Convergence of fields time (left) with $q = 0, 1, 2$ and space (right) with $p = 0, 1, 2$ for (49).

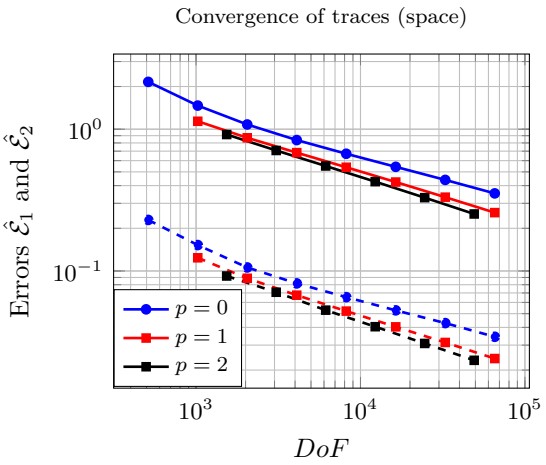

Figure 16: Convergence of trace variables space with $p = 0, 1, 2$ (right) for solution (50). Solid lines refer to error $\hat{\mathcal{E}}_1$ and dashed lines to error $\hat{\mathcal{E}}_2$.

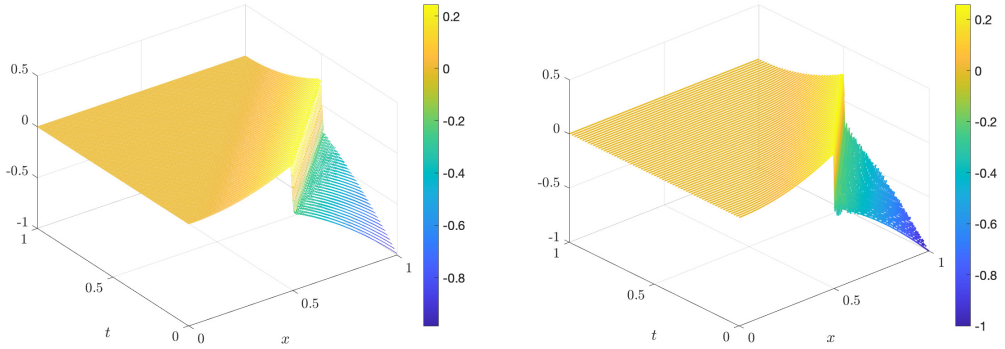

Figure 17: Approximation of fields and traces for solution (50) with $q = 0$ and $p = 2$.

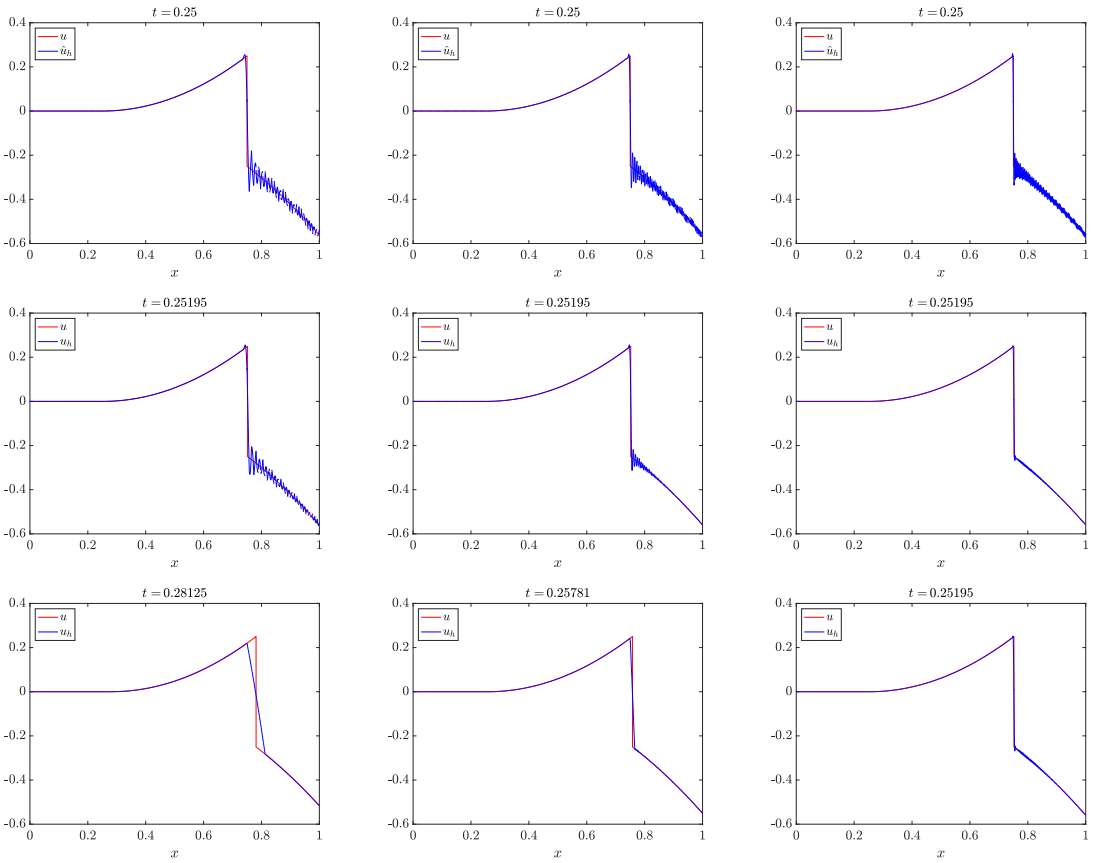

Figure 18: Convergence of traces in space (first row), convergence of fields in space (second row), convergence of fields in time (third row) for solution (50).

7. Conclusions and future work

In this work, we present a methodology to combine a semidiscretization in space by the DPG method together with the DPG-based time marching scheme. We proceed in two steps in the spirit of the method of lines. We first consider a broken ultraweak variational formulation in space and we introduce interface variables in space that are time-dependent. We then define two types of optimal test functions, corresponding to fields and traces, respectively, that symmetrize the operator in space. We additionally require the optimal test functions corresponding to traces to be orthogonal to the mass matrix in order to obtain a practical method in the context of exponential integrators. After statically condensing the traces in space we obtain a system of ODEs. Finally, considering an ultraweak variational formulation in time and introducing traces in time that are space-dependent we define the DPG-based time marching scheme. Here, the optimal test functions in space are approximate while the optimal test functions in time are analytical. We study the performance of our method for several 1D+time advection-reaction problems.

Possible future research lines include the extension of the proposed method to higher dimensions in space and other transient (semi-)linear problems together with the use of an error representation function to perform adaptive refinements in space. In particular, we are interested in the extension of this work to the Vlasov equation, which can require up to six phase-space dimensions. For a p-order method, the cost of sum-factorized matrix assembly is $O(p^{2d+1})$; so-called matrix-free approaches can compute the action of the matrix on a vector at a cost of $O(p^{d+1})$ (see [2, Table 1]). Recently, Deka and Einkemmer have developed a matrix-free exponential integrator for resistive MHD [7]. Given the potential cost savings in high dimensions, we would like to develop a matrix-free exponential integrator analogous to the one in the present work.

Appendix A. Computing matrix $K^T G^{-1} M$ for pure advection problem

In this section, we see that matrix $K^T G^{-1} M$ is singular for the pure advection case ($b = 1,\ c = 0$) when we select the adjoint graph norm. It is sufficient to show it for the master element $(0, 1)$ and lowest order Legendre polynomials: order 0 for trial and order 1 for test so we have

$$\mathcal{U}_h = \text{span}\{1\},\ \ \mathcal{V}_h = \text{span}\{1, 2x - 1\}.$$

If we select the adjoint graph norm 26, we obtain

$$K = \begin{bmatrix} 0 \\ -2 \end{bmatrix},\ \ M = \begin{bmatrix} 1 \\ 0 \end{bmatrix},\ \ G = \begin{bmatrix} 1 & 0 \\ 0 & \frac{13}{3} \end{bmatrix},$$

and therefore, $K^T G^{-1} M = 0$. Alternatively, if we select the localizable adjoint norm defined in (27), the Gramm matrix becomes

$$G = \begin{bmatrix} 1 & 1 \\ 1 & 5 \end{bmatrix},$$

and in this case $K^T G^{-1} M = \frac{1}{2}$. This results generalizes to any polynomial order p so in practice, for the transport equation we select norm (27).

Appendix B. Optimal testing for time-dependent traces

We now compute the optimal test functions corresponding to time-dependent traces $\bar{u}(t)$. For simplicity, we consider a single ODE ($s = 1$) and a master element in time ($m = T = 1$). The generalization to a general number or elements and to systems of ODEs is straightforward. In (21), we have an ODE coupled with an algebraic equation

$$\begin{cases} u'(t) + \lambda u(t) + \mu \bar{u}(t) = f_1(t),\ \forall t \in [0, 1], \\ \alpha u(t) + \beta \bar{u}(t) = f_2(t), \\ u(0) = u_0. \end{cases} \tag{B.1}$$

We multiply each equation by a test function $\{v_1, v_2\}$ and we integrate by parts the first one. Adding both equations we obtain

$$\int_0^1 u(-v_1' + \lambda v_1 + \alpha v_2)dt + \hat{u}v_1(1) + \int_0^1 \bar{u}(\mu v_1 + \beta v_2)dt = u_0 v_1(0) + \int_0^1 (f_1 v_1 + f_2 v_2)dt, \quad \text{(B.2)}$$

where $\hat{u}$ denotes the value of u at $t = 1$ and is treated as another unknown. We know from [32] that the analytical optimal test functions from the DPG method satisfy the adjoint equation, i.e.,

$$\begin{cases} -v_1'(t) + \lambda v_1(t) + \alpha v_2(t) = u(t), \ \forall t \in [0,1], \\ \mu v_1(t) + \beta v_2(t) = \bar{u}(t), \\ v_1(1) = \hat{u}. \end{cases} \quad \text{(B.3)}$$

Solving for v_2 in the second equation of (B.3), $v_2(t) = \beta^{-1}(\bar{u}(t) - \mu v_1(t))$, and substituting in the first equation, we obtain

$$\begin{cases} -v_1'(t) + \gamma v_1(t) = u(t) - \alpha\beta^{-1}\bar{u}(t), \ \forall t \in [0,1], \\ v_1(1) = \hat{u}, \end{cases} \quad \text{(B.4)}$$

where $\gamma = \lambda - \alpha\beta^{-1}\mu$. Therefore, for each trial function $(\hat{u}, u, \bar{u})$, we have the corresponding optimal test functions

$$\begin{cases} v_1(t) = e^{\gamma(t-1)}\hat{u} + e^{\gamma t}\displaystyle\int_t^1 e^{-\gamma s}(u(s) - \alpha\beta^{-1}\bar{u}(s))ds, \\ v_2(1) = \beta^{-1}(\bar{u}(t) - \mu v_1(t)). \end{cases} \quad \text{(B.5)}$$

Now, we compute the optimal test functions corresponding to piecewise polynomials in time for the trial space where we select the following basis

$$\{(1,0,0), (0,t^r,0), (0,0,t^{\bar{r}}), \ r = 0,\dots,q, \ \bar{r} = 0,\dots,\bar{q}\},$$

so we approximate the trial functions as

$$u(t) \approx \sum_{i=0}^{q} u_i t^i, \quad \bar{u}(t) \approx \sum_{j=0}^{\bar{q}} \bar{u}_j t^j.$$

- The optimal test functions corresponding to $(1,0,0)$ are

  $$\hat{v}_1(t) = e^{\gamma(t-1)}, \quad \hat{v}_2(t) = -\beta^{-1}\mu\hat{v}_1(t),$$

  and substituting into (B.2), we obtain

  $$\hat{u} = u_0\hat{v}_1(0) + \int_0^1 (f_1(t) - \beta^{-1}\mu f_2(t))\hat{v}_1(t)dt,$$

  which is equivalent to the first equation in (34).

- Integrating by parts (B.5) we obtain that the optimal test functions for $(0, t^r, 0)$ are given by the following recurrence formula

$$v_1^r(t) = e^{\gamma t}\int_t^1 e^{-\gamma s}s^r ds = \gamma^{-1}(t^r + r v_1^{r-1}(t) - \hat{v}_1(t)),\;\; v_2^r(t) = -\beta^{-1}\mu v_1^r(t),$$

and the system to compute the field variables is

$$\sum_{i=0}^{q} u_i \int_0^1 t^{i+r}dt = u_0 v_1^r(0) + \int_0^1 (f_1(t) - \beta^{-1}\mu f_2(t))v_1^r(t)dt,\;\; \forall r = 0, \dots, q.$$

which is equivalent to the second equation in (34).

- The optimal test functions for $(0, t^{\bar{r}}, 0)$ are

$$\bar{v}_1^{\bar{r}}(t) = -e^{\gamma t}\int_t^1 e^{-\gamma s}\alpha\beta^{-1}s^{\bar{r}}ds = -\gamma^{-1}(\alpha\beta^{-1}t^{\bar{r}} + \bar{r}\bar{v}_1^{\bar{r}-1}(t) - \hat{v}_1(t)\alpha\beta^{-1}),$$
$$\bar{v}_2^{\bar{r}}(t) = \beta^{-1}t^{\bar{r}} - \beta^{-1}\mu\bar{v}_1^{\bar{r}}(t),$$

and we get the following system of equations

$$\sum_{j=0}^{\bar{q}} \bar{u}_j \int_0^1 t^{j+\bar{r}}dt = u_0\bar{v}_1^{\bar{r}}(0) + \int_0^1 \beta^{-1}t^{\bar{r}}f_2(t)dt + \int_0^1 (f_1(t) - \beta^{-1}\mu f_2(t))\bar{v}_1^{\bar{r}}(t)dt,$$
$$\forall \bar{r} = 0, \dots, \bar{q}.$$

In conclusion, by considering directly an ultraweak variational formulation in (21) we recover the time-marching scheme (34) and an additional system to compute the time-dependent interface variables $\bar{u}(t)$. Here, as the analytical optimal test functions satisfy the adjoint equation, they decouple the fields from the traces in the time-marching scheme. We introduce $\bar{u}$ as a mathematical tool to consider broken test spaces the space variable but in practice, we only compute the field variables u and the traces in time $\hat{u}$.

Acknowledgements

Judit Muñoz-Matute has received founding from the European Union's Horizon 2020 research and innovation program under the Marie Sklodowska-Curie individual fellowship No. 101017984 (GEODPG) and the grant agreement No. 777778 (MATHROCKS), the Projects of the the Spanish Ministry of Science and Innovation with references PID2019-108111RB-I00 (FEDER/AEI) and PDC2021-121093-I00, the "BCAM Severo Ochoa" accreditation of excellence (SEV-2017-0718), the Basque Government through the BERC 2018-2021 program, and the Consolidated Research Group MATHMODE (IT1294-19) given by the Department of Education.

Leszek Demkowicz was partially supported with NSF grant No. 1819101 and partially supported by Sandia LDRD Project No. 218322.

Nathan V. Roberts was supported by Sandia LDRD Project No. 218322. Sandia National Laboratories is a multimission laboratory managed and operated by National Technology & Engineering Solutions of Sandia, LLC, a wholly owned subsidiary of Honeywell International Inc., for the U.S. Department of Energy's National Nuclear Security Administration under contract DE-NA0003525. This paper describes objective technical results and analysis. Any subjective views or opinions that might be expressed in the paper do not necessarily represent the views of the U.S. Department of Energy or the United States Government.

References

[1] A. H. Al-Mohy and N. J. Higham. Computing the action of the matrix exponential, with an application to exponential integrators. *SIAM Journal on Scientific Computing*, 33(2):488–511, 2011.

[2] R. Anderson, J. Andrej, A. Barker, J. Bramwell, J.-S. Camier, J. Cerveny, V. Dobrev, Y. Dudouit, A. Fisher, T. Kolev, W. Pazner, M. Stowell, V. Tomov, I. Akkerman, J. Dahm, D. Medina, and S. Zampini. Mfem: A modular finite element methods library. *Computers & Mathematics with Applications*, 81:42–74, 2021. Development and Application of Open-source Software for Problems with Numerical PDEs.

[3] C. Bacuta, L. Demkowicz, J. Mora, and C. Xenophontos. Analysis of non-conforming DPG methods on polyhedral meshes using fractional Sobolev norms. *Computers & Mathematics with Applications*, 95:215–241, 2021.

[4] H. Berland, B. Skaflestad, and W. M. Wright. EXPINT—A MATLAB package for exponential integrators. *ACM Transactions on Mathematical Software (TOMS)*, 33(1):4–es, 2007.

[5] C. Carstensen, L. Demkowicz, and J. Gopalakrishnan. Breaking spaces and forms for the DPG method and applications including Maxwell equations. *Computers & Mathematics with Applications*, 72(3):494–522, 2016.

[6] J. Chan, N. Heuer, T. Bui-Thanh, and L. Demkowicz. A robust DPG method for convection-dominated diffusion problems II: Adjoint boundary conditions and mesh-dependent test norms. *Computers & Mathematics with Applications*, 67(4):771–795, 2014.

[7] P. J. Deka and L. Einkemmer. Exponential integrators for resistive magnetohydrodynamics: Matrix-free leja interpolation and efficient adaptive time stepping. *The Astrophysical Journal Supplement Series*, 259(2):57, apr 2022.

[8] L. Demkowicz and J. Gopalakrishnan. A class of discontinuous Petrov–Galerkin methods. Part I: The transport equation. *Computer Methods in Applied Mechanics and Engineering*, 199(23-24):1558–1572, 2010.

[9] L. Demkowicz and J. Gopalakrishnan. Analysis of the DPG method for the Poisson equation. *SIAM Journal on Numerical Analysis*, 49(5):1788–1809, 2011.

[10] L. Demkowicz and J. Gopalakrishnan. A class of discontinuous Petrov–Galerkin methods. Part II: Optimal test functions. *Numerical Methods for Partial Differential Equations*, 27(1):70–105, 2011.

[11] L. Demkowicz and J. Gopalakrishnan. An overview of the discontinuous Petrov–Galerkin method. In *Recent developments in discontinuous Galerkin finite element methods for partial differential equations*, pages 149–180. Springer, 2014.

[12] L. Demkowicz, J. Gopalakrishnan, and B. Keith. The DPG-star method. *Computers & Mathematics with Applications*, 79(11):3092–3116, 2020.

[13] L. Demkowicz, J. Gopalakrishnan, I. Muga, and J. Zitelli. Wavenumber explicit analysis of a DPG method for the multidimensional Helmholtz equation. *Computer Methods in Applied Mechanics and Engineering*, 213:126–138, 2012.

[14] L. Demkowicz, J. Gopalakrishnan, S. Nagaraj, and P. Sepúlveda. A spacetime DPG method for the Schrödinger equation. *SIAM Journal on Numerical Analysis*, 55(4):1740–1759, 2017.

[15] L. Demkowicz, J. Gopalakrishnan, and A. H. Niemi. A class of discontinuous Petrov–Galerkin methods. Part III: Adaptivity. *Applied numerical mathematics*, 62(4):396–427, 2012.

[16] L. Demkowicz and N. Heuer. Robust DPG method for convection-dominated diffusion problems. *SIAM Journal on Numerical Analysis*, 51(5):2514–2537, 2013.

[17] L. Demkowicz and N. Roberts. The DPG method for the convection–reaction problem, revisited. Technical Report 21-05, Oden Report, 2021.

[18] L. Diening and J. Storn. A space-time DPG method for the heat equation. *Computers & Mathematics with Applications*, 105:41–53, 2022.

[19] T. Ellis, J. Chan, and L. Demkowicz. Robust DPG methods for transient convection-diffusion. In *Building bridges: connections and challenges in modern approaches to numerical partial differential equations*, pages 179–203. Springer, 2016.

[20] T. Ellis, L. Demkowicz, J. Chan, and R. Moser. Space-time DPG: Designing a method for massively parallel CFD. ICES report. *The Institute for Computational Engineering and Sciences, The University of Texas at Austin*, pages 14–32, 2014.

[21] T. Führer, N. Heuer, and J. S. Gupta. A time-stepping DPG scheme for the heat equation. *Computational Methods in Applied Mathematics*, 17(2):237–252, 2017.

[22] T. Führer, N. Heuer, and M. Karkulik. Analysis of backward Euler primal DPG methods. *Computational Methods in Applied Mathematics*, 21(4):811–826, 2021.

[23] J. Gopalakrishnan and P. Sepúlveda. A space-time DPG method for the wave equation in multiple dimensions. *Space-Time Methods. Applications to Partial Differential Equations*, pages 129–154, 2017.

[24] S. Henneking and L. Demkowicz. A numerical study of the pollution error and DPG adaptivity for long waveguide simulations. *Computers & Mathematics with Applications*, 95:85–100, 2021.

[25] M. Hochbruck and A. Ostermann. Exponential integrators. *Acta Numerica*, 19:209–286, 2010.

[26] M. Hochbruck and A. Ostermann. Exponential multistep methods of Adams-type. *BIT Numerical Mathematics*, 51(4):889–908, 2011.

[27] M. Hochbruck, A. Ostermann, and J. Schweitzer. Exponential Rosenbrock-type methods. *SIAM Journal on Numerical Analysis*, 47(1):786–803, 2009.

[28] J. Li and L. Demkowicz. An Lp-DPG method for the convection–diffusion problem. *Computers & Mathematics with Applications*, 95:172–185, 2021.

[29] C. Moler and C. Van Loan. Nineteen dubious ways to compute the exponential of a matrix, twenty-five years later. *SIAM review*, 45(1):3–49, 2003.

[30] J. Muñoz-Matute, L. Demkowicz, and D. Pardo. Error representation of the time-marching DPG scheme. *Computer Methods in Applied Mechanics and Engineering*, 391:114480, 2022.

[31] J. Muñoz-Matute, D. Pardo, and L. Demkowicz. A DPG-based time-marching scheme for linear hyperbolic problems. *Computer Methods in Applied Mechanics and Engineering*, 373:113539, 2021.

[32] J. Muñoz-Matute, D. Pardo, and L. Demkowicz. Equivalence between the DPG method and the exponential integrators for linear parabolic problems. *Journal of Computational Physics*, 429:110016, 2021.

[33] J. Niesen and W. M. Wright. Algorithm 919: A Krylov subspace algorithm for evaluating the φ-functions appearing in exponential integrators. *ACM Transactions on Mathematical Software (TOMS)*, 38(3):1–19, 2012.

[34] S. Petrides and L. Demkowicz. An adaptive multigrid solver for DPG methods with applications in linear acoustics and electromagnetics. *Computers & Mathematics with Applications*, 87:12–26, 2021.

[35] N. V. Roberts, T. Bui-Thanh, and L. Demkowicz. The DPG method for the Stokes problem. *Computers & Mathematics with Applications*, 67(4):966–995, 2014.

[36] N. V. Roberts and S. Henneking. Time-stepping DPG formulations for the heat equation. *Computers & Mathematics with Applications*, 95:242–255, 2021.

[37] W. E. Schiesser. *The numerical method of lines: integration of partial differential equations*. Elsevier, 2012.